Crystal Growth, Thermoelectric Properties, and Electronic Structure of $AgBi_3S_5$ and $AgSb_xBi_{3-x}S_5$ ($x = 0.3$)

Jun-Ho Kim,[†] Duck-Young Chung,[†] Daniel Bilc,[‡] Sim Loo,[§] Jarrod Short,[§] Subhendra D. Mahanti,[‡] Tim Hogan,[§] and Mercouri G. Kanatzidis*[,†]

Departments of Chemistry, Physics and Astronomy, and Electrical and Computer Engineering, Michigan State University, East Lansing, Michigan 48824

Received February 8, 2005. Revised Manuscript Received April 28, 2005

The compound $AgBi_3S_5$ (**I**) (synthetic pavonite) and its solid solution $AgSb_xBi_{3-x}S_5$ ($x = 0.3$) (**II**) were prepared by direct combination of elemental Ag, Bi, Sb, and S. They crystallize in the monoclinic space group $C2/m$ with $a = 13.345(3)$ Å, $b = 4.0416(8)$ Å, $c = 16.439(3)$ Å, and $\beta = 94.158(3)°$ for **I** and $a = 13.302(4)$ Å, $b = 4.0381(11)$ Å, $c = 16.388(5)$ Å, and $\beta = 94.347(5)°$ for **II**. The Bridgman technique was used to grow bulk crystals of these materials. The crystal structure refinements, physicochemical properties, and thermoelectric properties of these materials are presented. The thermoelectric power for $AgBi_3S_5$ and $AgSb_{0.3}Bi_{2.7}S_5$ showed −64 and −98 μV/K, respectively, with room-temperature electrical conductivity of 489 and 260 S/cm. The thermal conductivity for both compounds at room temperature was measured to be very low at ∼1 W/m·K, respectively. Electronic band structure calculations for $AgBi_3S_5$ suggest the importance of silver d-states to the charge transport and also indicate the presence of an indirect energy gap.

Introduction

Bismuth chalcogenide chemistry has been extensively studied since the $Bi_2Te_{3-x}Se_x$ and $Bi_{2-x}Sb_xTe_3$ alloys showed high thermoelectric (TE) figures of merit ZT.[1,2] In recent years, intense efforts focused on discovering new thermoelectric materials have been devoted to the class of ternary and quaternary alkali metal bismuth chalcogenides. From the chemistry standpoint this class of materials has proven to be remarkably large and has contributed many complex compositions and structures favorable for high TE performance.[3] Some examples include $CsBi_4Te_6$,[4] β-$K_2Bi_8Se_{13}$,[5] $K_{2.5}Bi_{8.5}Se_{14}$,[5] $BaBiTe_3$,[6] $K_{1-x}Sn_{5-x}Bi_{11+x}Se_{22}$,[7] $A_{1+x}M_{4-2x}Bi_{7+x}Se_{15}$ (A = K, Rb; M = Sn, Pb),[8] $A_2Bi_8Se_{13}$ (A = Rb, Cs),[9] $CsMBi_3Te_6$, and $CsM_2Bi_3Te_7$ (M = Pb, Sn).[10] Recently, a silver-containing compound, $Ag_{1-x}Pb_{18}SbTe_{20}$,[11] showed a large figure of merit (ZT) of ∼2 at 800 K.

In comparison to the selenides and tellurides, most of the alkali metal bismuth sulfides exhibit wide energy band gaps and strong ionic interactions between the alkali metal ions and the $[Bi_xS_y]^{z-}$ framework. For example, the alkali metal containing β-,γ-$CsBiS_2$,[12] γ-$RbBi_3S_5$,[13] KBi_3S_5,[14] $KBi_{6.33}S_{10}$,[15] and $K_2Bi_8S_{13}$[15] show band gaps of ∼1.1−1.4 eV. In general, these gaps are wider than what is considered to be optimum for TE performance because the pertinent materials tend to be exceedingly resistive. Instead, desirable energy gaps for TE applications up to 1000 °C are thought to be less than ∼0.6 eV. To include the bismuth sulfide class of materials in TE investigations, it is preferable to produce systems with smaller semiconductor gaps. One way to do so is to replace, partially or totally, the alkali metals with other less electro-

* To whom correspondence should be addressed.
[†] Department of Chemistry.
[‡] Department of Physics and Astronomy.
[§] Department of Electrical and Computer Engineering.

(1) $ZT = S^2\sigma T/\kappa$, where S is the Seebeck coefficient, σ is the electrical conductivity, T is the temperature, and κ is the thermal conductivity, which includes electron and phonon contributions.
(2) *CRC Handbook of Thermoelectric Materials*; Rowe, D. M., Ed.; CRC Press: Boca Raton, FL, 1995.
(3) (a) Kanatzidis, M. G. *Semicond. Semimet.* **2001**, *69*, 51−100. (b) Chung, D.-Y.; Iordanidis, L.; Choi, K.-S.; Kanatzidis, M. G. *Bull. Korean Chem. Soc.* **1998**, *19*, 1283−1293. (c) Kanatzidis, M. G.; Mahanti, S. D.; Hogan, T. P. *Chemistry, Physics and Materials Science of Thermoelectric Materials: Beyond Bismuth Telluride*; Kluwer Academic/Plenum Publishers.: New York, 2003; p 35. (d) Mrotzek, A.; Kanatzidis, M. G. *Acc. Chem. Res.* **2003**, *36*, 111−119.
(4) Chung, D-. Y.; Hogan, T.; Brazis, P. W.; Kannewurf, C. R.; Bastea, M.; Uher, C.; Kanatzidis, M. G. *Science* **2000**, *287*, 1024−1027.
(5) Chung, D.-Y.; Choi, K.-S.; Iordanidis, L.; Schindler, J. L.; Brazis, P. W.; Kannewurf, C. R.; Chen, B.; Hu, S.; Uher, C.; Kanatzidis, M. G. *Chem. Mater.* **1997**, *9*, 3060−3071.
(6) Chung, D.-Y.; Jobic, S.; Hogan, T.; Kannewurf, C. R.; Brec, R.; Rouxel, J.; Kanatzidis, M. G. *J. Am. Chem. Soc.* **1997**, *119*, 2505−2515.
(7) Mrotzek, A.; Chung, D.-Y.; Hogan, T.; Kanatzidis, M. G. *J. Mater. Chem.* **2000**, *10*, 1667−1672.
(8) Choi, K.-S.; Chung, D.-Y.; Mrotzek, A.; Brazis, P.; Kannewurf, C. R.; Uher, C.; Chen, W.; Hogan, T.; Kanatzidis, M. G. *Chem. Mater.* **2001**, *13* (3), 756−764.
(9) Iordanidis, L.; Brazis, P. W.; Kyratsi, T.; Ireland, J.; Lane, M.; Kannewurf, C. R. Chen, W.; Dyck, J. S.; Uher, C.; Ghelani, N. A.; Hogan, T.; Kanatzidis, M. G. *Chem. Mater.* **2001**, *13*, 622−633.
(10) Hsu, K.-F.; Chung, D.-Y.; Lal, S.; Mrotzek, A.; Kyratsi, T.; Hogan, T.; Kanatzidis M. G. *J. Am. Chem. Soc.* **2002**, *124*, 2410−2411.
(11) Hsu, K.-F.; Loo, S.; Guo, F.; Chen, W.; Dyck, J. S.; Uher, C.; Hogan, T.; Polychroniadis, E. K.; Kanatzidis, M. G. *Science* **2004**, *303*, 818−821.
(12) McCarthy, T. J.; Ngeyi, S.-P.; Liao, J.-H.; DeGroot, D.; Hogan, T.; Kannewurf, C. R.; Kanatzidis, M. G. *Chem. Mater.* **1993**, *5*, 331−340.
(13) Iordanidis, L.; Bilc, D.; Mahanti, S. D.; Kanatzidis, M. G. *J. Am. Chem. Soc.* **2003**, *125*, 13741.
(14) McCarthy, T. J.; Tanzer, T. A.; Kanatzidis, M. G. *J. Am. Chem. Soc.* **1995**, *117*, 1294−1301.
(15) (a) McCarthy, T. J.; Tanzer, T. A.; Chen, L. H.; Iordanidis, L.; Hogan, T.; Kannewurf, C. R.; Uher, C.; Chen, B.; Kanatzidis, M. G. *Chem. Mater.* **1996**, *8*, 1465−1474. (b) Chen, B.; Uher, C.; Iordanidis, L.; Kanatzidis, M. G. *Chem. Mater.* **1997**, *9*, 1655−1658.

10.1021/cm0502931 CCC: $30.25
Published on Web 06/14/2005

positive metals capable of stronger interactions with the $[Bi_xS_y]^{z-}$ framework such as Ag^+. This is the reason we examined $AgBi_3S_5$. The known Ag/Bi/S compounds exhibit a variety of structural types and compositions.[16] These include $AgBiS_2$,[17] $AgBi_6S_9$,[18] $Ag_3Bi_7S_{12}$,[19] and $AgBi_3S_5$[20] which have not been studied with respect to their physicochemical and charge transport properties.

Herein we report new results on the synthetic pavonite, $AgBi_3S_5$, and its derivative $AgSb_xBi_{3-x}S_5$ ($x = 0.3$) and evaluate their potential as thermoelectric materials. The crystal structure refinements, crystal growth, physicochemical properties, band structure calculations, and exceptionally low thermal conductivity of these materials are presented.

Experimental Section

Reagents. Chemicals were used as obtained: bismuth chunks (99.999% Noranda, Canada), sulfur powder (sublimed, Spectrum Chemical Mfg. Corp., Gardena, CA), and antimony shot form (99.9%, Noranda, Canada)

Ag Powder. A silver coin (99.999%) was dissolved in nitric acid. The solution was neutralized to a pH of 7 with ammonium hydroxide. Sodium borohydride was added to reduce the Ag ions to a black precipitate of Ag metal powder. The precipitate of silver was filtered, washed thoroughly with water, and dried in a vacuum oven at 150 °C. The obtained fine powder of Ag was identified by powder X-ray diffraction.

Synthesis. The products are air- and water-stable and all manipulations were carried out in air. For all compounds the yield was quantitative. The purity and homogeneity of the products were verified by comparing the X-ray powder diffraction patterns to those calculated by the crystallographically determined atomic coordinates.

$AgBi_3S_5$. A mixture of Ag powder (1.294 g, 12 mmol), Bi (7.523 g, 36 mmol), and S (2.024 g, 63 mmol) was loaded in a fused silica tube (13 mm diameter) and subsequently flame-sealed at a residual pressure of $<10^{-4}$ mbar. The tube was carefully placed in a flame of natural gas-oxygen torch until the mixture was well molten. The tube was removed from the flame and allowed to solidify in air. A metallic black polycrystalline ingot of $AgBi_3S_5$ was obtained. A quantitative microprobe analysis using energy dispersive spectroscopy (EDS) was performed on a scanning electron microscope (SEM) on several single crystals of $AgBi_3S_5$ which gave the approximate composition of $Ag_{0.95}Bi_{3.30}S_5$. To grow highly oriented crystal specimens for the thermoelectric property measurements, the product was ground and loaded in a silica tube (13 mm diameter) with a point end and sealed under vacuum. The tube was heated to 800 °C in a Bridgman furnace and descended at a rate of 3.25 mm/h through a sharp (100 °C/cm) temperature gradient.[21] A pure and well-oriented ingot (35 mm long, 11 mm diameter) of $AgBi_3S_5$ was obtained.

$AgSb_{0.3}Bi_{2.7}S_5$. A mixture of elemental Ag powder (1.294 g, 12 mmol), Sb (0.438 g, 3.6 mmol), Bi (6.771 g, 32.4 mmol), and S (2.024 g, 63 mmol) was loaded in a fused silica tube (13 mm diameter) and subsequently flame-sealed at a residual pressure of $<10^{-4}$ mbar. The mixture was carefully molten with a natural gas-oxygen torch as above. After quenching in air, a black silvery polycrystalline ingot of $AgSb_{0.3}Bi_{2.7}S_5$ was obtained. SEM/EDS analysis on several single crystals of $AgSb_{0.3}Bi_{2.7}S_5$ showed the approximate composition of $Ag_{0.93}Sb_{0.2}Bi_{3.45}S_5$. The Bridgman technique was used to obtain highly oriented crystalline ingots of $AgSb_{0.3}Bi_{2.7}S_5$ using the same conditions as $AgBi_3S_5$.

Physical Measurements

Electron Microscopy. Quantitative microprobe analysis for the compounds was performed with a JEOL JSM-6400V scanning electron microscope (SEM) equipped with a Noran Vantage energy dispersive spectroscopy (EDS) detector. Data were collected for 30 s using an accelerating voltage of 20 kV. All reported results are an average of measurements on at least three different crystals.

Differential Thermal Analysis. Differential thermal analysis (DTA) was performed with a computer-controlled thermal analyzer (Shimadzu DTA-50). Twenty milligrams of ground crystals was sealed in a silica ampule under vacuum. A silica ampule containing the equal mass of alumina was placed on the reference side of the detector. The sample was heated to the desired temperature at 10 °C/min, isothermed for 2 min, and then cooled at 10 °C/min. The heating program was recycled to check reproducibility of the thermal behavior of the sample. The reported melting point is the peak temperature. After DTA, the sample was examined by powder X-ray diffraction to identify if any decomposed product formed during heating/cooling cycles.

Solid-State UV/Vis Spectroscopy. Optical diffuse reflectance measurement was made at room temperature with a Shimazu UV-3101 PC double-beam, double-monochromator spectrometer operating in the 200−2500 nm region. The instrument was equipped with an integrating sphere and controlled by a personal computer. $BaSO_4$ powder was used as reference (100% reflectance). Absorption data were calculated from the reflectance data using the Kubelka−Munk function.[22]

Charge Transport and Thermal Conductivity Measurements. A four-sample measurement system was used to simultaneously measure electrical conductivity, thermoelectric power, and thermal conductivity.[23] To fully characterize the figure of merit, the properties were measured for each sample over the selective temperature range of interest (system capability is 4.2−475 K). To alleviate offset error voltages and increase the density of data points, a slow-ac technique was used with a heater pulse period of 720 s.[24] The pulse shape was monitored, in situ, to determine temperature stabilization, and the sample chamber was maintained at a pressure less than 10^{-5} Torr for the entire measurement run. A rectangular sample with dimensions 3 mm × 3 mm × 5 mm was mounted in the standard four-probe configuration for the thermal conductivity, and the heater current was adjusted for an average temperature gradient of 1 K. The sample stage and radiation shield were gold-coated copper to minimize radiation effects and to maintain temperature uniformity. However, the thermal conductivity data obtained are still subject to radiation loss effects due to the relatively long shape of the samples. All electrical leads were 25 μm in diameter with lengths greater than 10 cm to minimize thermal conduction losses. Data acquisition and computer control of the

(16) Makovicky, E. *Neues Jahrb. Mineral., Abh.* **1989**, *160*, 269−297.
(17) (a) Wernick, J. H. *Am. Mineral.* **1960**, *45*, 591−598. (b) Wernick, J. H. *J. Mater. Sci.* **1968**, *3*, 498−501.
(18) Mumme, W. G. *Neues Jahrb. Mineral.* **1990**, 193−204.
(19) Herbert, H. K.; Mumme, *W. G. Neues Jahrb. Mineral.* **1981**, 69−80.
(20) Makovicky, E.; Mumme, W. G.; Watts, J. A. *Can. Mineral.* **1977**, *15*, 339−348.
(21) Kyratsi, T.; Chung, D.-Y.; Choi, K.-S.; Dick, J. S.; Chen, W.; Uher, C.; Kanatzidis, M. G. *Mater. Res. Soc. Symp. Proc.* **2000**, *626*, Z8.8.1−Z8.8.6.
(22) Kubelka−Munk function: $\alpha/S = (1 - R)^2/2R$, where α is the absorption coefficient, S is the scattering coefficient, and R is the reflectance at a given wavenumber.
(23) Hogan, T.; Ghelani, N.; Loo, S.; Sportouch, S.; Kim, S.-J.; Chung, D.-Y. Kanatzidis, M. G. *Proc. Int. Conf. Thermoelectr.* **1999**, 671−674.
(24) Maldonado, O. *Cryogenics* **1992**, *32*, 908−912.

Table 1. Crystallographic Data for Synthesized $AgBi_3S_5$ and $AgSb_{0.34}Bi_{2.66}S_5$ and Previous $AgBi_3S_5$

empirical formula	$AgBi_3S_5$	$AgSb_{0.34}Bi_{2.66}S_5$	$AgBi_3S_5$ from ref 19
formula weight	895.11	865.23	
temperature	293(2) K	293(2) K	
crystal system	monoclinic	monoclinic	monoclinic
space group	*C*2/*m*	*C*2/*m*	*C*2/*m*
unit cell dimensions	$a = 13.345(3)$ Å	13.302(4) Å	13.305(2) Å
	$b = 4.0416(8)$ Å	4.0381(11) Å	4.042(1) Å
	$c = 16.439(3)$ Å	16.388(5) Å	16.417(2) Å
	$\beta = 94.158(3)°$	94.347(5)°	94.0(0)°
volume	884.3(3) Å^3	877.8(4) Å^3	880.7 Å^3
Z	4	4	4
density (calculated)	6.723 mg/m^3	6.547 mg/m^3	6.74(5) mg/m^3
absorption coefficient	62.791 mm^{-1}	57.456 mm^{-1}	
F(000)	1504	1460	
crystal size	0.04 × 0.42 × 0.03 mm^3	0.02 × 0.18 × 0.16 mm^3	
theta range for data collection	2.48 to 28.22°	2.49 to 28.14°	
index ranges	$-17 \le h \le 17$	$-16 \le h \le 17$	
	$-5 \le k \le 5$	$-5 \le k \le 5$	
	$-21 \le l \le 21$	$-21 \le l \le 19$	
reflections collected	3778	3675	
independent reflections	1147 [R(int) = 0.0295]	1137 [R(int) = 0.0423]	
completeness to theta = 28.22°	92.1%	92.8%	
refinement method		full-matrix least-squares on F^2	
data/restraints/parameters	1147/0/58	1137/0/59	
goodness-of-fit on F^2	1.137	1.092	
final R indices [$I > 2\sigma(I)$]	R1[a] = 0.0301, wR2 = 0.0807	R1 = 0.0400, wR2 = 0.1118	0.110
R indices (all data)	R1[a] = 0.0317, wR2 = 0.0814	R1 = 0.0442, wR2 = 0.1137	
extinction coefficient	0.00098(8)		
largest diff. peak and hole	3.209 and −2.669 e. Å^{-3}	2.734 and −4.549 e. Å^{-3}	

[a] $R1 = \Sigma||F_o| - |F_c||/\Sigma|F_o|$. $wR2 = \{\Sigma[w(F_o^2 - F_c^2)^2]/\Sigma[w(F_o^2)^2]\}^{1/2}$.

system were maintained under the LabVIEW[25] software environment. For higher temperature measurements of thermoelectric power and electrical conductivity, a single sample measurement system with system capabilities up to 800 K was used.[26] This system utilizes single-ended thermocouples for concurrently monitoring the temperature gradient and voltage gradient on the sample, and it also utilizes the slow pulsing technique described above.

To obtain the thermal conductivity from 300 to 800 K, we measured the thermal diffusivity (α) using the laser flash technique. The thermal conductivity (κ) values were calculated as a product of these quantities, i.e., $\kappa = \alpha C_p d$, where C_p is the specific heat and d is the sample's density. A plot of the specific heat is given in the Supporting Information. The bulk density (d) values were calculated from the sample's geometry and mass (12 mm in diameter and 2.3 mm thick) and the specific heat (C_p) was measured on a 12 mm in diameter and 1.0 mm thick sample using differential scanning calorimetry.[27]

Powder X-ray Diffraction. A calibrated CPS 120 INEL X-ray powder diffractometer equipped with a position-sensitive detector, operating at 40 kV/25 mA with a flat geometry and employing graphite monochromatized Cu Kα radiation was used to obtain powder patterns of starting materials and all products.

Single-Crystal X-ray Crystallography. A Bruker SMART Platform CCD diffractometer was used for data collection at room temperature. The individual frames were measured with an omega angle rotation of 0.3° and an acquisition time of 30 s for each crystal. The SMART[28] software was used for the data acquisition and SAINT[28] software for data extraction and reduction. An analytical absorption correction was performed using face indexing and the program XPREP in the SAINT software package, followed by a semiempirical absorption correction based on symmetrically equivalent reflections with the program SADABS.[28] Structural solution and refinements were successfully done using the SHELXTL[28] package of crystallographic programs. The structures were solved with direct methods.

Table 2. Atomic Coordinates and Equivalent Isotropic Displacement Parameters (Å^2 × 10^3) for $AgBi_3S_5$

	x	*y*	*z*	*U*(eq)[a]	occupancy
Bi(1)	0.7392(1)	0.0000	0.1110(1)	20(1)	1
Bi(2)	0.9740(1)	−0.5000	0.2165(1)	21(1)	1
Bi(3)	0.2198(1)	0.0000	0.3894(1)	25(1)	1
Ag(1)	0.0000	0.0000	0.0000	40(1)	1
Ag(2)	0.0000	−0.5000	0.5000	30(1)	1
S(1)	0.8625(2)	−0.5000	0.0551(2)	19(1)	1
S(2)	0.8426(3)	0.0000	0.2590(2)	19(1)	1
S(3)	0.5992(3)	−0.5000	0.1519(3)	35(1)	1
S(4)	0.0768(3)	−0.5000	0.3617(2)	23(1)	1
S(5)	0.1508(2)	0.0000	0.5338(2)	16(1)	1

[a] *U*(eq) is defined as one-third of the trace of the orthogonalized $\mathbf{U}_{ij}$ tensor.

The data collection was performed by selecting the crystals from the interior of the Bridgman-grown ingots. The complete data collection parameters, details of the structure solution, and refinement for $AgBi_3S_5$ and $AgSb_{0.3}Bi_{2.7}S_5$ are given in Table 1 and compared with the previously reported data for $AgBi_3S_5$.[20] The fractional coordinates and temperature factors (U_{eq}) of all the atoms with estimated standard deviations are given in Tables 2 and 3.

The previously reported structure for pavonite, $AgBi_3S_5$, was determined using intensity data from integrated Weissenberg photographs and X-ray powder diffraction. The structure solution was accomplished using the *h*0*l* data to construct a Patterson function $\rho(u,0,w)$, which gave $R = 11\%$ from 510 reflections. In contrast, the new refinement for the synthetic $AgBi_3S_5$ provides significantly more accurate atomic coordinates, and bond lengths and angles and much lower R values (3−4%) from >3000 reflections.

Band Structure Calculation. The electronic structure calculations were performed using the self-consistent full-potential linearized augmented plane wave method (LAPW)[29] within density functional theory (DFT),[30] using the generalized gradient ap-

(25) *LabVIEW*, Version 5.0; National Instruments: Austin, TX, 1999.
(26) Loo, S.; Short, J.; Hsu, K.-F.; Kanatzidis, M. G.; Hogan, T. *Mater. Res. Soc. Symp. Proc.* **2004**, *793*, S9.4.1-9.
(27) The high-temperature thermal conductivity measurements for a well-grown polycrystalline ingot sample of $AgBi_3S_5$ were accomplished by Thermophysical Properties Research Laboratory inc., West Lafayette, IN 47906, U.S.A. (www.tprl.com/).
(28) *SMART, SAINT, SHELXTL: Data Collection and Processing Software for the SMART-CCD system*; Siemens Analytical X-ray Instruments Inc.: Madison, WI, 1997.

Table 3. Atomic Coordinates and Equivalent Isotropic Displacement Parameters ($Å^2 \times 10^3$) for $AgSb_{0.34}Bi_{2.66}S_5$

	x	*y*	*z*	*U*(eq)[a]	occupancy
Bi(1)/Sb(1)	0.7389(1)	0.0000	0.1116(1)	20(1)	0.871(4)/0.129
Bi(2)/Sb(2)	0.4732(1)	0.0000	0.2171(1)	20(1)	0.785(4)/0.215
Bi(3)	0.7192(1)	−0.5000	0.3892(1)	26(1)	1
Ag(1)	0.5000	−0.5000	0.0000	25(1)	1
Ag(2)	0.5000	0.0000	0.5000	29(1)	1
S(1)	0.8643(3)	−0.5000	0.0542(3)	22(1)	1
S(2)	0.8438(3)	0.0000	0.2586(3)	21(1)	1
S(3)	0.6017(4)	−0.5000	0.1529(4)	34(1)	1
S(4)	0.5764(3)	0.0000	0.3615(3)	22(1)	1
S(5)	0.6514(3)	−0.5000	0.5333(3)	16(1)	1

[a] *U*(eq) is defined as one-third of the trace of the orthogonalized $\mathbf{U}_{ij}$ tensor.

proximation (GGA) of Perdew, Burke, and Ernzerhof[31] for the exchange and correlation potential. The values of the atomic radii were taken to be 2.3 au for Ag and S atoms and 2.6 au for Bi atoms, where au is the atomic unit (0.529 Å). Convergence of the self-consistent iterations was performed for 20 k points inside the irreducible Brillouin zone to within 0.0001 Ry with a cutoff of −6.0 Ry between the valence and the core states. Scalar relativistic corrections were included and spin−orbit interaction was incorporated using a second variational procedure.[32] The calculations were performed using the WIEN2K program.[33] It is necessary to use the more accurate atomic coordinates obtained by the new refinement to achieve meaningful results in the DFT calculations.

Results and Discussion

Synthesis and Crystal Growth. $AgBi_3S_5$ and $AgSb_xBi_{3-x}S_5$ were synthesized by reacting the elemental mixtures (Ag:Bi:S = 1:3:5.25, Ag:Sb:Bi:S = 1:*x*:3−*x*:5.25) in a torch flame. A slight excess of S was added to compensate for a loss of sulfur vaporized from the top surface of the molten mixture during the reaction. The $AgSb_xBi_{3-x}S_5$ series of compounds with several *x* values (up to $x = 1$) were investigated. The $AgSb_xBi_{3-x}S_5$ with $x = 0.1$, 0.2, 0.3, and 0.5 produced pure solid solutions, while the $x = 1$ provided a mixture of the $AgSb_xBi_{3-x}S_5$ solid solution and Bi_2S_3. This is not surprising since $AgSb_3S_5$ (i.e., $x = 3$) is not a stable compound. $AgBi_3S_5$ and $AgSb_{0.3}Bi_{2.7}S_5$ appear to melt congruently at 735 and 723 °C, respectively (see DTA in Supporting Information). For both compounds a comparison of the X-ray powder diffraction patterns before and after the DTA experiments showed no significant phase change.

For thermal and electrical conductivity measurements we grew large crystals of $AgBi_3S_5$ and $AgSb_{0.3}Bi_{2.7}S_5$ using the Bridgman technique. The obtained ingots show well-grown highly oriented characteristics, Figure 1. The natural crystal habit of these compounds is to grow as long planks and in the ingots the long axis (crystallographic *b*-axis) lies parallel to the Bridgman translation axis. These ingots were cut along the direction parallel and perpendicular to the crystal growth.

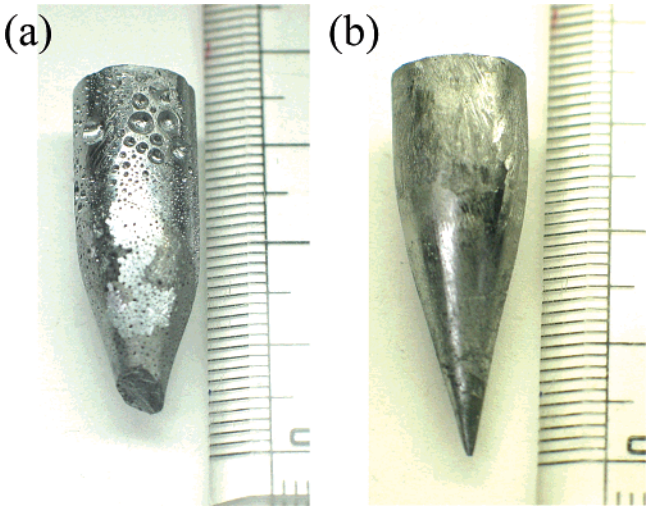

Figure 1. Ingots of (a) $AgBi_3S_5$ and (b) $AgSb_{0.3}Bi_{2.7}S_5$ grown in a Bridgman furnace.

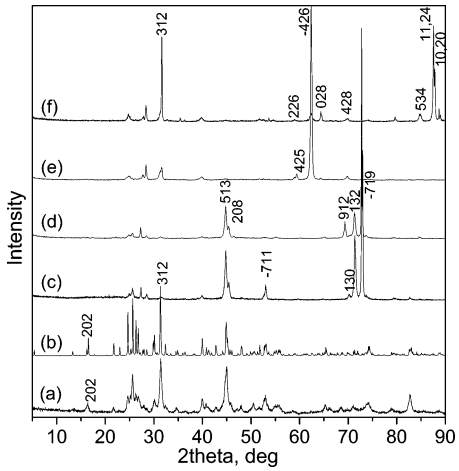

Figure 2. XRD patterns of $AgBi_3S_5$ (a) of polycrystalline powdered sample, (b) calculated from the crystal structure, (c) well-grown ingot sample with the X-ray beam along the *a* direction on an *ab* plane, (d) *b* direction on an *ab* plane, (e) *b* direction on a *bc* plane, and (f) *c* direction on a *bc* plane.

Experimental evidence for a very high degree of crystal orientation achieved in the ingots was obtained from X-ray diffraction data taken on cut specimens along different directions, Figure 2. The presence of a certain class of reflections when the X-ray beam is incident along one direction (e.g., (*h*2*l*) in Figure 2f) and their complete absence when the beam is incident along a perpendicular direction (e.g., in Figure 2d) is proof that a nearly perfect (estimated at >96%) crystallographic orientation has been achieved.

Structure Description. $AgBi_3S_5$ has a strongly anisotropic three-dimensional framework composed of two types of slabs which can be described as an assembly of blocks excised from the cubic NaCl structure type. These blocks are two-dimensional slabs excised by slicing the NaCl lattice perpendicular to the [311] direction, Figure 3.

The thinner slab (Slab I) is composed of a single [AgS_6] octahedron sandwiched by two square pyramids of [BiS_5]. The thicker slab (Slab II) is made of a distorted galena-type structure[34] with one [AgS_6] and four [BiS_6] octahedra per one diagonal octahedral chain. The two slabs are intercon-

(29) Singh, D. *Planewaves, Pseudopotentials, and the LAPW method*; Kluwer Academic: Boston, 1994.
(30) Hohenberg, P.; Kohn, W. *Phys. Rev.* **1964**, *136*, B864. Kohn, W.; Sham, L. *Phys. Rev.* **1965**, *140*, A1133.
(31) Perdew, J. P.; Burke, K.; Ernzerhof, M. *Phys. Rev. Lett.* **1996**, *77*, 3865.
(32) Koelling, D. D.; Harmon, B. *J. Phys. C* **1980**, *13*, 6147.
(33) Blaha, P.; Schwarz, K.; Madsen, G.; Kvasnicka, D.; Luitz, J. *WIEN2K, An Augmented Plane Wave + Local Orbitals Program for Calculating Crystal Properties*; Schwarz, K., Ed.; Vienna University of Technology: Vienna, Austria, 2001.
(34) Takeuchi, Y.; Takagi, J.; Yamanaka, T. *Z. Kristallogr. Bd.* **1974**, *140*, 249.

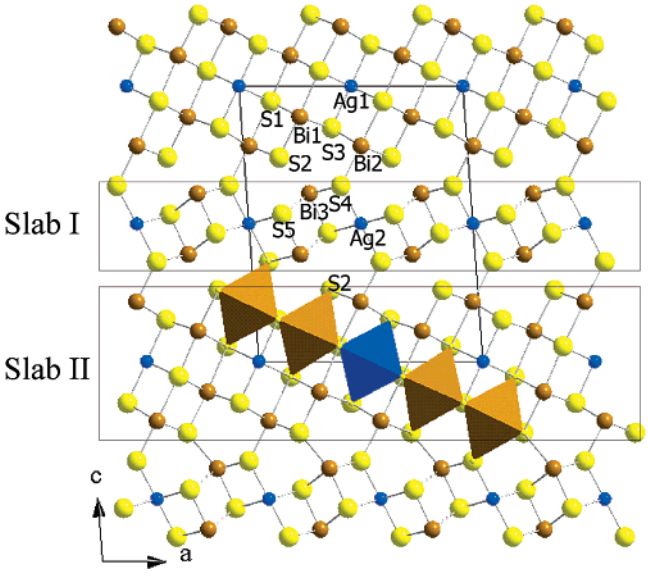

Figure 3. Projection of the structure of $AgBi_3S_5$ down the *b*-axis. Two slabs can be described by slightly distorted layers cut along the (311) face of the NaCl-type structure. The slab (II) includes five octahedra per one diagonal octahedral chain. In the structure of $AgSb_{0.3}Bi_{2.7}S_5$ the Bi(1) and Bi(2) sites are disordered with Sb atoms.

nected through sharing atom S(4). This modular construction gives the compound a highly anisotropic morphology and electronic structure.

The structure has three crystallographically independent Bi atoms. Bi(1) is in a slightly distorted octahedral site with distances from 2.708(3) to 2.959(3) Å to the coordinated S atoms. Bi(2) is also in an octahedral site of sulfur atoms with bonding distance from 2.664(4) to 2.947(3) Å. Bi(3) is in Slab I and has five normal covalent bonds with neighboring S atoms at a square pyramidal coordination (Sb_2Se_3-type) and two additional longer interactions with S(2) atoms in Slab II at 3.445(3) Å; namely, Bi(3) has one bond with S(5) at 2.609(3) Å, two bonds with S(4) atoms at 2.795(3) Å, and two bonds with S(5) at 2.888(2) Å. Ag(1) sits in a slightly distorted octahedral site in Slab II with two Ag(1)−S(3) bonds at 2.741(6) Å and four Ag(1)−S(1) bonds at 2.917(2) Å. Ag(2) is in a flattened octahedral site with four Ag(2)−S(5) bonds at 2.877(2) Å and two short Ag(2)−S(4) bonds at 2.560(4) Å, Figure 4. Even though the S(4) atoms serve as bridges between the two slabs and the Ag(2)−S(4) and Bi(2)−S(4) bond distances are shorter, (see Table 4 and Figure 4), the equivalent isotropic displacement parameters of Ag atoms are relatively larger. It can be rationalized if we consider that there may be some rattling of Ag atoms going in the large octahedral pockets. A low-temperature data

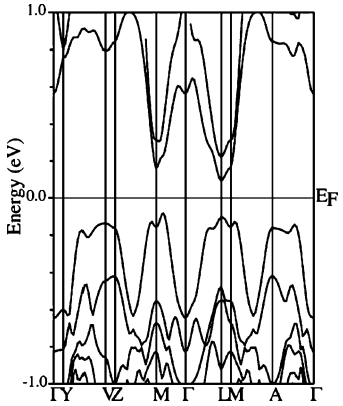

Figure 5. Electronic band structure of $AgBi_3S_5$ with spin−orbit interaction included (E_g = 0.17 eV).

collection on $AgBi_3S_5$ may show Ag atoms settling into the sides of the octahedron.

All members of the solid solutions $AgSb_xBi_{3-x}S_5$ are isostructural to $AgBi_3S_5$. In $AgSb_{0.3}Bi_{2.7}S_5$ the Sb atoms occupy two bismuth sites, Bi(1) and Bi(2), on the Slab II with 13% and 21%, respectively. The structure of $AgSb_{0.3}Bi_{2.7}S_5$ has slightly smaller unit cell parameters than $AgBi_3S_5$ because of Sb substitution, Table 1. This shrinks the room available for all metals compared with $AgBi_3S_5$ and at the same time achieves optimum packing. Especially the equivalent isotropic displacement parameters of Ag(1) and Ag(2) are much smaller than those of $AgBi_3S_5$, which indicates less rattling of Ag atoms, Tables 3 and 4.

Energy Gaps and Electronic Band Structure Calculations. Electronic band structure calculations can be an important tool to explore the properties of materials. It not only can rationalize the observed properties but also can provide guidance for further modifications toward a desired direction. To the best of our knowledge, band structure calculations on $AgBi_3S_5$ (pavonite) have not been reported. Thus, we first carried out electronic band structure calculations to understand the influence of the crystal structure on the electronic structure and properties of $AgBi_3S_5$ and $AgSb_{0.3}Bi_{2.7}S_5$. We also examined how each element contributes to the conduction band and valence band structure near the Fermi energy level.

Electronic structure calculations show that $AgBi_3S_5$ is an indirect narrow band-gap semiconductor with an energy gap of ∼0.17 eV, Figures 5 and 6A. Density of states (DOS) analysis shows that the high valence band states in the range from −0.75 to 0 eV consist mostly of p states of S(4) and S(5) atoms which are hybridized with d states of Ag(2), Figure 6C and D. This suggests a two-dimensional hole

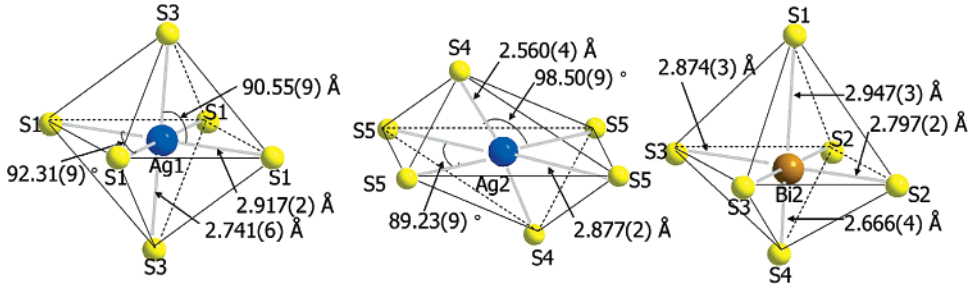

Figure 4. A scheme of the local coordination environment of Ag(1), Ag(2), and Bi(2) atoms in $AgBi_3S_5$.

Table 4. Bond Lengths [Å] and Angles [°] for $AgBi_3S_5$ and $AgSb_{0.34}Bi_{2.66}S_5$

$AgBi_3S_5$				$AgSb_{0.34}Bi_{2.66}S_5$			
Bi(1)−S(2)	2.708(3)	S(2)−Bi(2)−S(3)	172.73(14)	M(1)[a]−S(2)	2.691(4)	S(2)−M(2)−S(3)	172.88(16)
Bi(1)−S(1)	2.803(2) × 2	S(2)−Bi(2)−S(3)	88.63(7)	M(1)−S(1)	2.825(3) × 2	S(2)−M(2)−S(3)	88.63(8)
Bi(1)−S(3)	2.865(3) × 2	S(3)−Bi(2)−S(3)	89.36(11)	M(1)−S(3)	2.837(3) × 2	S(3)−M(2)−S(3)	88.43(12)
Bi(1)−S(1)	2.959(3)	S(4)−Bi(2)−S(1)	179.36(11)	M(1)−S(1)	2.950(4)	S(4)−M(2)−S(1)	178.27(13)
		S(2)−Bi(2)−S(1)	86.55(8)			S(2)−M(2)−S(1)	87.15(10)
Bi(2)−S(4)	2.666(4)	S(3)−Bi(2)−S(1)	86.35(12)	M(2)−S(4)	2.644(4)	S(3)−M(2)−S(1)	86.19(14)
Bi(2)−S(2)	2.797(2) × 2			M(2)−S(2)	2.771(3) × 2		
Bi(2)−S(3)	2.874(3) × 2	S(5)−Bi(3)−S(4)	82.28(10)	M(2)−S(3)	2.895(3) × 2	S(5)−Bi(3)−S(4)	82.44(11)
Bi(2)−S(1)	2.947(3)	S(4)−Bi(3)−S(4)	92.63(11)	M(2)−S(1)	2.940(4)	S(4)−Bi(3)−S(4)	92.91(12)
		S(5)−Bi(3)−S(5)	80.89(9)			S(5)−Bi(3)−S(5)	80.57(10)
Bi(3)−S(5)	2.609(3)	S(4)−Bi(3)−S(5)	163.08(11)	Bi(3)−S(5)	2.591(4)	S(4)−Bi(3)−S(5)	162.92(13)
Bi(3)−S(4)	2.795(3) × 2	S(4)−Bi(3)−S(5)	86.84(7)	Bi(3)−S(4)	2.786(3) × 2	S(4)−Bi(3)−S(5)	86.63(8)
Bi(3)−S(5)	2.888(2) × 2	S(5)−Bi(3)−S(5)	88.79(9)	Bi(3)−S(5)	2.885(3) × 2	S(5)−Bi(3)−S(5)	88.84(11)
Ag(1)−S(3)	2.741(6) × 2	S(3)−Ag(1)−S(3)	180.00(11)	Ag(1)−S(3)	2.756(6) × 2	S(3)−Ag(1)−S(3)	180.00(13)
Ag(1)−S(1)	2.917(2) × 4	S(3)−Ag(1)−S(1)	89.45(9)	Ag(1)−S(1)	2.893(3) × 4	S(3)−Ag(1)−S(1)	90.24(10)
		S(3)−Ag(1)−S(1)	90.55(9)			S(3)−Ag(1)−S(1)	89.76(10)
Ag(2)−S(4)	2.560(4) × 2	S(1)−Ag(1)−S(1)	180	Ag(2)−S(4)	2.556(5) × 2	S(1)−Ag(1)−S(1)	180.00(16)
Ag(2)−S(5)	2.877(2) × 4	S(1)−Ag(1)−S(1)	87.69(9)	Ag(2)−S(5)	2.875(3) × 4	S(1)−Ag(1)−S(1)	88.52(11)
		S(1)−Ag(1)−S(1)	92.31(9)			S(1)−Ag(1)−S(1)	91.48(11)
S(2)−Bi(1)−S(1)	91.25(8)	S(1)−Ag(1)−S(1)	180.00(16)	S(2)−M(1)−S(1)	91.08(10)		
S(1)−Bi(1)−S(1)	92.27(10)			S(1)−M(1)−S(1)	91.24(12)	S(4)−Ag(2)−S(4)	180
S(2)−Bi(1)−S(3)	95.01(12)	S(4)−Ag(2)−S(4)	180	S(2)−M(1)−S(3)	94.93(14)	S(4)−Ag(2)−S(5)	98.69(10)
S(1)−Bi(1)−S(3)	88.67(7)	S(4)−Ag(2)−S(5)	98.50(9)	S(1)−M(1)−S(3)	88.70(8)	S(4)−Ag(2)−S(5)	81.31(10)
S(1)−Bi(1)−S(3)	173.65(13)	S(4)−Ag(2)−S(5)	81.50(9)	S(1)−M(1)−S(3)	173.99(16)	S(5)−Ag(2)−S(5)	180
S(3)−Bi(1)−S(3)	89.71(11)	S(5)−Ag(2)−S(5)	180.00(13)	S(3)−M(1)−S(3)	90.73(13)	S(5)−Ag(2)−S(5)	90.77(10)
S(2)−Bi(1)−S(1)	176.69(10)	S(4)−Ag(2)−S(5)	98.50(9)	S(2)−M(1)−S(1)	176.50(12)	S(5)−Ag(2)−S(5)	89.23(10)
S(1)−Bi(1)−S(1)	86.47(8)	S(5)−Ag(2)−S(5)	89.23(9)	S(1)−M(1)−S(1)	86.47(10)	S(4)−Ag(2)−S(5)	81.31(10)
S(3)−Bi(1)−S(1)	87.32(12)	S(5)−Ag(2)−S(5)	90.77(9)	S(3)−M(1)−S(1)	87.52(14)		
		S(4)−Ag(2)−S(5)	81.50(8)				
S(4)−Bi(2)−S(2)	93.89(9)	S(4)−Ag(2)−S(5)	98.50(8)	S(4)−M(2)−S(2)	94.03(11)		
S(2)−Bi(2)−S(2)	92.50(10)	S(5)−Ag(2)−S(5)	180	S(2)−M(2)−S(2)	93.55(12)		
S(4)−Bi(2)−S(3)	93.19(13)			S(4)−M(2)−S(3)	92.57(14)		

[a] M = Bi/Sb.

transport in Slab I since S(4), S(5), and Ag(2) atoms are located in it. The bottom of the conduction band consists of p states of Bi(1) and Bi(2) atoms with very small contribution from Bi(3) atoms, Figure 6B. The Bi(1) and Bi(2) p states are hybridized with the p states of S(1), S(2), and S(3) atoms in the range from 0 to 1 eV, suggesting that the electron transport is mostly confined within Slab II. Therefore, the electron and hole transports should be separated in space.

From the projected density of states calculations (Figure 6D) we find that the filled d-states of Ag(1) and Ag(2) lie surprisingly high in energy and in the same region as the S p bands. This results in a strong mixing of the Ag d states and the S p states and leads to two a rather narrow hybridized valence band. Due to the different local environments of Ag(1) and Ag(2), the Ag(2) associated band is about 0.75 eV higher than the Ag(1) associated band. As a result the top of the valence band and hence the hole transport takes place in Slab I in which the Ag(2) atom resides, Figure 3. The narrow valence band leads to a rapidly increasing density of states near the valence band maximum, which suggests that if this system could be hole-doped, it could show a very large thermopower. It will be interesting to test this prediction by making hole-doped samples.

Furthermore, the mixing of the Bi p states with these hybridized Ag−S states leads to splitting of the p bands near the conduction band bottom associated with different Bi atoms (Figure 6B). The splitting of Bi p bands is due to the energy level repulsion between the bottom of the conduction band Bi p states and the top of the valence band Ag−S hybridized states. The energy level repulsion increases with decreasing separation between the energy levels. Since the Ag(2)−S states are higher in energy than the Ag(1)−S states, the separation of the energy levels between the Ag(2)−S states and Bi(3) p states is smaller than that of Ag(1)−S states and Bi(1) and Bi(2) p states. The Bi(3) p states have a stronger repulsion and these states are pushed above the Bi(1) and Bi(2) p states. As a result, the bottom of the conduction band has primarily Bi(1) and Bi(2) p character and the resulting electron carriers move predominantly in Slab II, as discussed in the previous paragraph. Clearly, the Ag atoms play a very important role (although indirect) in determining the nature of the states near the band gap region. In this regard the Ag systems greatly differ from their alkali counterparts. In the K systems the K d states are not present whereas in the Rb(Cs) systems the Rb(Cs) d states are much lower in energy (core states) than the S d states.[13]

The optical absorption properties of $AgBi_3S_5$ and $AgSb_{0.3}Bi_{2.7}S_5$ were examined with solid-state optical absorption spectroscopy. The spectra in the UV/Vis range show intense absorptions for both $AgBi_3S_5$ and $AgSb_{0.3}Bi_{2.7}S_5$ around 0.6 eV, Figure 7. The difference between calculation and measurement is not unusual because the LDA/GGA band calculation has a tendency to underestimate the gap energy.[35] The difference in the direct band gap (∼0.2 eV) and the optical gap (∼0.6 eV) can be due to a variety of reasons. We know that LDA/GGA band gaps tend to be smaller than the true band gaps and this may explain the discrepancy.[35] There is however another possibility. If we look at the total DOS (Figure 6A), we see that there is a sharp rise in the DOS of the conduction band at about 0.4−0.5 eV above the conduction band bottom. Absorption to these states may be

(35) Aulbur, W. E.; Jonsson, L.; Wilkins, J. W. *Solid State Phys.*; Ehrenreich, H., Spaepen, F., Eds.; Academic Press*:* New York, 2000; Vol. 54, p 11.

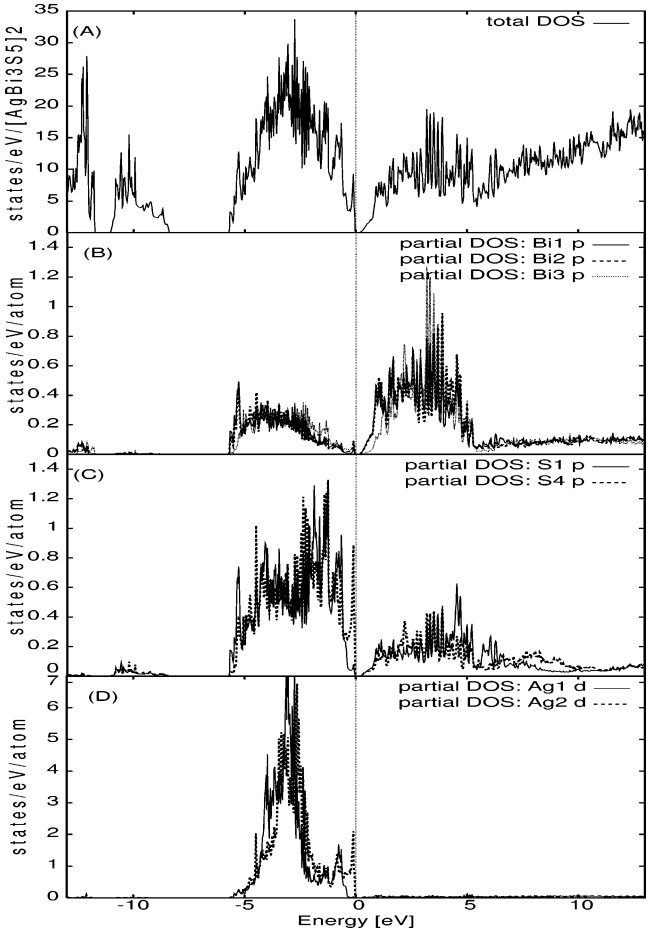

Figure 6. Density of states (DOS) of $AgBi_3S_5$. (A) Total DOS, partial atomic DOS of (B) bismuth atoms, (C) S1 and S4, and (D) silver atoms.

the origin of the observed optical absorption edge at ~0.6 eV. A careful calculation of the optical response function including the energy dependence of the optical matrix element will be able to shed light on this issue.

Thermoelectric Properties. Thermopower measurements on samples cut from oriented polycrystalline ingots were carried out along the crystal growth direction (i.e., crystallographic *b*-axis). The thermopower of $AgBi_3S_5$ is negative and increases almost linearly from -25 μV/K at 80 K to -160 μV/K at 700 K, Figure 8a and 9a. The negative value indicates that the predominant carriers are electrons (n-type), and charge transport in this compound is accomplished by carriers moving predominantly through Bi p orbitals near the conduction band bottom as suggested by the results of the electronic band calculations.

Electrical conductivity measurements were also performed along the direction of crystal growth. The conductivity of the $AgBi_3S_5$ ingot was relatively high and exhibited negative temperature dependence with the value decreasing almost linearly from 660 S/cm at 80 K to 134 S/cm at 700 K. This is a typical behavior for a degenerate semiconductor, Figure 8a. It is possible that the degree of doping varies in ingots of these materials since the electrical conductivities between two separate measurements at a low- and a high-temperature range showed approximately 100 S/cm gap at room temperature, Figures 8a and 9a. Variations in electrical conductivities were observed in the oriented ingot sample of $AgBi_3S_5$ screened by scanning probe conductivity[36] measurements at room temperature. The scanned electrical conductivity values varied from 244 S/cm at one crystal domain to almost twice the value, 415 S/cm, at another domain which was only 0.2 mm away.

Among the $AgSb_xBi_{3-x}S_5$ solid solutions the compound with $x = 0.3$ was selected for measuring charge transport properties. This material showed slightly lower electrical conductivity and higher thermopower than $AgBi_3S_5$, implying a lower number of carriers. The room-temperature values were 260 S/cm for the conductivity and -98 μV/K for the thermopower, Figure 8b. The thermopower of $AgSb_{0.3}Bi_{2.7}S_5$ increases almost linearly from -35 μV/K at 80 K to -150 μV/K at 400 K and the conductivity decreases from 344 S/cm at 80 K to ~200 S/cm at 400 K.

The thermal conductivity of $AgBi_3S_5$ was observed at ~1.5 W/m·K at room temperature and it increases as temperature rises from 80 to 300 K, Figure 8a. The thermal conductivity can be divided into two contributions, electronic κ_{ele} and lattice κ_{latt}.[37] Because the room temperature electronic conductivity is <300 S/cm, the electronic contribution is only a small fraction of the total and the lattice thermal conductivity dominates heat transport in these materials. The rising thermal conductivity with rising temperature observed in the data is due to significant radiative losses (which begin to appear around 200 K) inherent in the measurement. The thermal conductivity of $AgSb_{0.3}Bi_{2.7}S_5$ showed a similarly low value (~1.6 W/m·K) at room temperature to that of

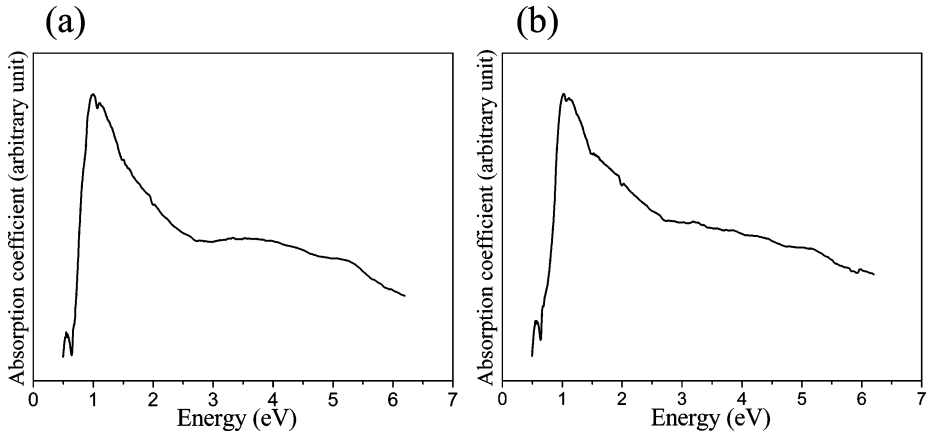

Figure 7. Solid-state UV/Vis absorption spectra for (a) $AgBi_3S_5$ and (b) $AgSb_{0.3}Bi_{2.7}S_5$.

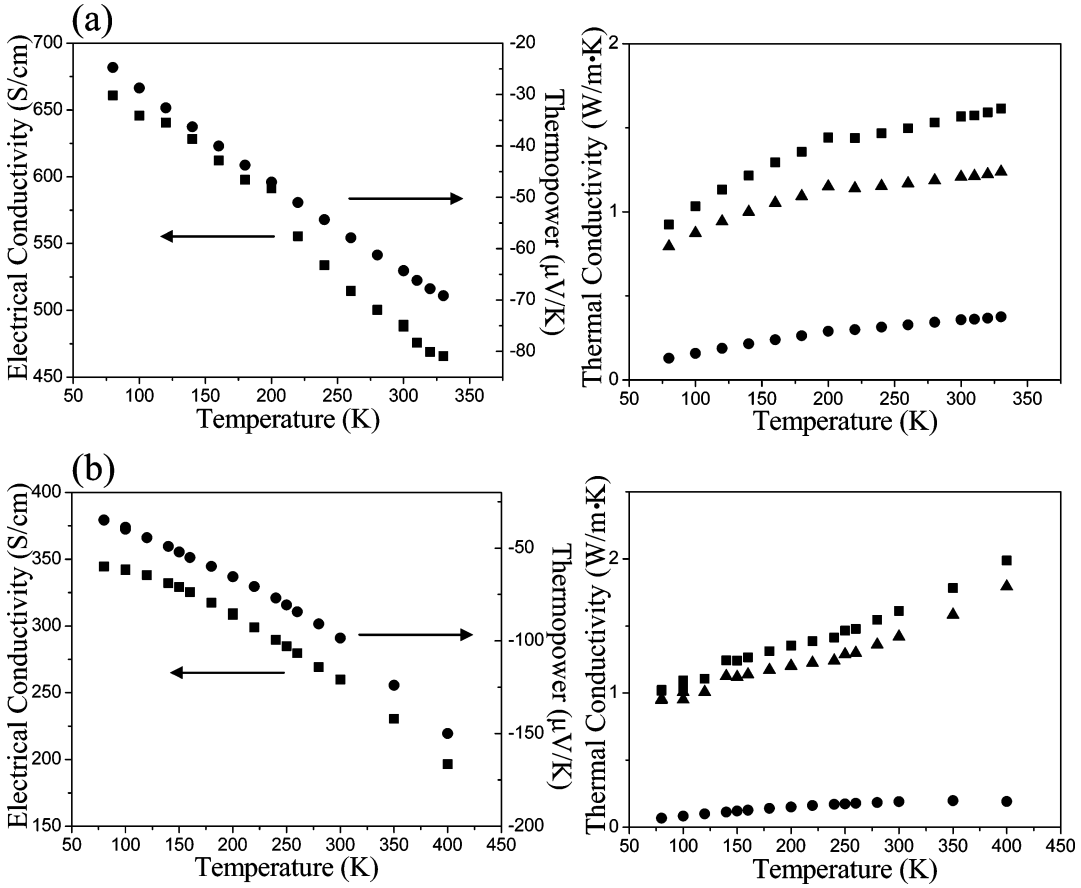

Figure 8. Variable temperature thermopower, electrical conductivity, and thermal conductivity for (a) $AgBi_3S_5$ and (b) $AgSb_{0.3}Bi_{2.7}S_5$. (■ = κ_{tot}, ● = κ_e, ▲ = κ_{latt}).

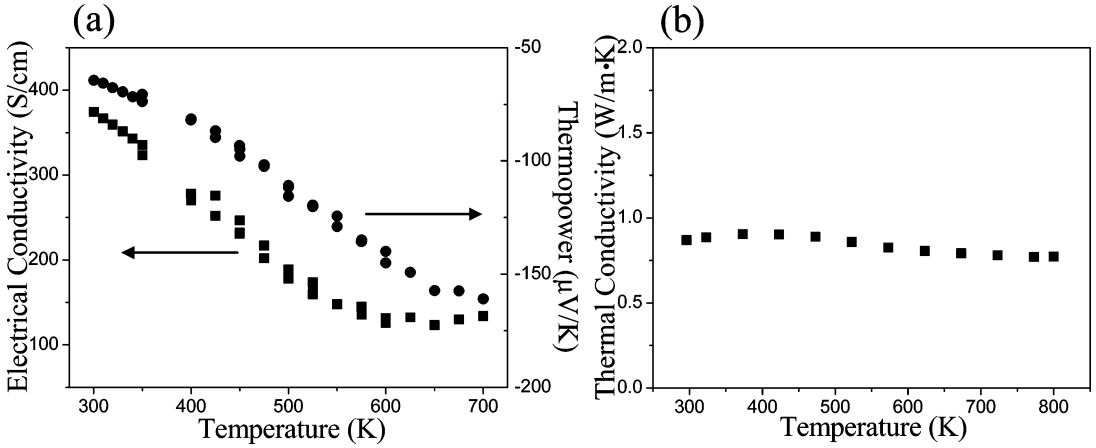

Figure 9. (a) Variable temperature thermopower and electrical conductivity data for $AgBi_3S_5$. (b) Thermal conductivity for $AgSb_{0.3}Bi_{2.7}S_5$ measured with the thermal diffusivity technique at high temperature.

$AgBi_3S_5$, Figure 8b. Radiation losses are evident in the measurement which raise the thermal conductivity.

A much more correct value of thermal conductivity was obtained (on $AgSb_{0.3}Bi_{2.7}S_5$) using a different method[27] (i.e., thermal diffusivity technique) that is not subject to radiation losses. These measurements actually showed a very low thermal conductivity of less than 1 W/m·K which did not change considerably with temperature, Figure 9b. In comparison with the room-temperature values obtained with the steady-state technique (Figure 8b), the observed difference of ~0.76 W/m·K is attributed to irradiative losses. At 800 K an exceptionally low value of 0.75 W/m·K is attained, Figure 9b. These values are consistent with the low crystal symmetry, complexity of the crystal structure, and the presence of heavy atoms (e.g., Bi) in the structure.

(36) The typical four-point probe method used for measuring the electrical conductivity utilizes two voltage leads at some fixed spacing. The scanning conductivity system translates one of the voltage leads along the length of the sample, and the corresponding slope of voltages collected versus distance scanned between voltages is used to calculate the electrical conductivity. If a discontinuity in the slope exists, this may indicate a change in the homogeneity of the material.

(37) The thermal conductivity is generally represented by the sum of electronic (κ_{ele}) and lattice (κ_{latt}) contributions. The κ_{latt} is estimated by the difference between total and electronic thermal conductivity calculated by the Wiedemann−Franz law. Kittel, C. *Introduction to Solid State Physics*, 7th ed.; John Wiley & Sons: New York, 1996; p 166.

The fact that the lattice thermal conductivities of $AgBi_3S_5$ and $AgSb_{0.3}Bi_{2.7}S_5$ are similar indicates a 10% participation of Sb atoms in the Bi atom sites of solid solution is not enough to cause a significant reduction in the lattice thermal conductivity in this system.

Concluding Remarks

The synthesis, crystal growth, thermoelectric properties of $AgBi_3S_5$, and its solid solution $AgSb_{0.3}Bi_{2.7}S_5$ and electronic band structure of $AgBi_3S_5$ were studied for the first time. Both $AgBi_3S_5$ and $AgSb_{0.3}Bi_{2.7}S_5$ show degenerate n-type semiconducting behavior with relatively high electrical conductivities and extremely low thermal conductivities. The electronic band structure calculation of $AgBi_3S_5$ suggests that the electron transport is mostly confined within Slab II. As the result of substitution of Sb in Slab II, the electrical conductivity is slightly reduced and thermopower increased but the thermal conductivity did not change significantly. This study emphasizes the importance of crystal growth for $AgBi_3S_5$. The calculations suggest that the silver d-states are involved near the Fermi level through hybridization with sulfur and influence the charge transport properties in this material. They also suggest a high thermopower in this system should p-type doping be achievable. The controlled substitution with other elements in the slabs of $AgBi_3S_5$ and modification of the structure by partially replacing Ag with alkali metal, copper, or thallium could help to further modulate the thermoelectric properties in this class of compounds.

Acknowledgment. Financial support from the Office of Naval Research is gratefully acknowledged.

Supporting Information Available: Figure plots of the specific heat and differential thermal analysis for $AgBi_3S_5$ and $AgSb_{0.3}Bi_{2.7}S_5$. Crystallographic information (CIF). This material is available free of charge via the Internet at http://pubs.acs.org.

CM0502931